Coaxial MoS₂@Carbon Hybrid Fibers: A Low-Cost Anode Material for High-Performance Li-Ion Batteries

Rui Zhou [1], Jian-Gan Wang [1,*], Hongzhen Liu [1], Huanyan Liu [1], Dandan Jin [1], Xingrui Liu [1], Chao Shen [1], Keyu Xie [1] and Bingqing Wei [1,2,*]

[1] State Key Laboratory of Solidification Processing, Center for Nano Energy Materials, School of Materials Science and Engineering, Northwestern Polytechnical University and Shaanxi Joint Lab of Graphene (NPU), Xi'an 710072, China; zhourui12@mail.nwpu.edu.cn (R.Z.); liuhongzhennwpu@outlook.com (H.L.); liuhuanyan@mail.nwpu.edu.cn (H.L.); jindandan0210@163.com (D.J.); liuxingrui@nwpu.edu.cn (X.L.); shenchao@nwpu.edu.cn (C.S.); kyxie@nwpu.edu.cn (K.X.)

[2] Department of Mechanical Engineering, University of Delaware, Newark, DE 19716, USA

* Correspondence: wangjiangan@nwpu.edu.cn (J.-G.W.); weib@udel.edu (B.W.); Tel.: +86-29-8846-0204 (J.-G.W.)

Abstract: A low-cost bio-mass-derived carbon substrate has been employed to synthesize MoS₂@carbon composites through a hydrothermal method. Carbon fibers derived from natural cotton provide a three-dimensional and open framework for the uniform growth of MoS₂ nanosheets, thus hierarchically constructing coaxial architecture. The unique structure could synergistically benefit fast Li-ion and electron transport from the conductive carbon scaffold and porous MoS₂ nanostructures. As a result, the MoS₂@carbon composites—when serving as anodes for Li-ion batteries—exhibit a high reversible specific capacity of 820 mAh·g⁻¹, high-rate capability (457 mAh·g⁻¹ at 2 A·g⁻¹), and excellent cycling stability. The use of bio-mass-derived carbon makes the MoS₂@carbon composites low-cost and promising anode materials for high-performance Li-ion batteries.

Keywords: MoS₂; composite; anode; low cost; Li-ion battery

1. Introduction

The worsening environmental problems and energy crisis have accelerated the development of electric vehicles and portable electronics, which forward an ever-growing demand for lithium-ion batteries (LIBs) with high energy density and excellent rate capability [1,2]. Among the LIB components, the commercial anode material of graphite suffers from low theoretical specific capacity (i.e., 372 mAh·g⁻¹), slow reaction kinetics, and possible safety issues resulting from its low discharge voltage (<0.2 V) that may cause the formation of lithium dendrites [3–5]. Therefore, it is imperative to explore a high-performance anode material that can serve as an alternative replacement of the graphite-based anode [6–8].

In recent years, two-dimensional (2D) graphene-like nanomaterials such as transition metal dichalcogenides (TMDs) have shown great potential for their applications in energy conversion and storage fields [9–12]. As a typical TMD, MoS₂ possesses a layered structure analogous to graphite, and is composed of S-Mo-S layers separated by Van der Waals interactions [13–15]. The unique structure is favorable for reversible Li⁺ insertion/extraction, thus rendering high theoretical specific capacity (670 mAh·g⁻¹), which is almost double that of graphite's [16,17]. However, the practical application of MoS₂ is still hindered by its poor cycling stability and inferior rate performance due to

its intrinsically low electronic conductivity and the possible structural destruction during repeated charge–discharge processes [18].

To overcome these drawbacks, combining nanostructured MoS_2 with conductive and flexible materials has been demonstrated to be an effective approach to improve the electrochemical performance. Carbon materials with large specific surface area and excellent electronic conductivity—such as graphene, carbon nanotubes, carbon nanofibers, carbon spheres, etc.—are considered to be ideal substrates in this respect [15,19–21]. MoS_2/graphene hybrid nanoflowers were developed via a simple hydrothermal method, and delivered a specific capacity of 1150 mAh·g^{-1} after 60 cycles [22]. Single-layered ultrasmall nanoplates of MoS_2 embedded in carbon nanofibers was used as the anode of LIBs, and showed a good cycling capability of 661 mAh·g^{-1} after 1000 cycles [23]. Compared with pure MoS_2 counterparts, the improved lithium storage performance can be ascribed to the synergistic effect of carbon and MoS_2 nanostructures. It should be noted that the fabrication of these carbon substrates is extremely time-consuming and costly, which would limit their widespread implementation. Moreover, non-uniform MoS_2 aggregations on the carbon backbone is another obstacle to achieving a maximum utilization of active materials [24,25]. Therefore, it remains a big challenge to explore a cost-effective MoS_2-based anode material with excellent electrochemical performance.

In this work, we report the use of a bio-mass-derived carbon substrate from low-cost natural cotton for subsequent growth of MoS_2 nanosheets. The carbon fiber substrate provides not only a three-dimensional (3D) and open framework for homogeneous deposition of nanostructured MoS_2, but also high electrical conductivity to improve the electrochemical reaction kinetics of MoS_2. The as-prepared MoS_2@carbon anode material delivers high specific capacity, excellent rate capability, and long cycling stability. Moreover, the bio-mass-derived-carbon simplifies the fabrication process, making the MoS_2@carbon composite serve as a cost-effective anode material for high-performance LIBs.

2. Results and Discussion

The crystalline structure of the as-prepared materials was investigated by X-ray diffraction (XRD). As shown in Figure 1a, both MoS_2@carbon and pure MoS_2 exhibit similar XRD profiles. The distinct diffraction peaks with 2θ at around 14°, 33°, 39°, 49°, 59°, and 60° correspond to the (002), (100), (103), (105), (008), and (107) crystal planes of MoS_2 with 2H phase, respectively [26–28]. Raman spectra were recorded to further elucidate the component and structure of the MoS_2@carbon composite (Figure 1b). It is clearly revealed that the two distinct peaks at around 374 and 406 cm^{-1} can be ascribed to the in-plane E^1_{2g} and out-of-plane A_{1g} modes of the hexagonal MoS_2 crystal, respectively [29,30]. In addition, the two broad Raman peaks located at 1350 and 1583 cm^{-1} are readily assigned to the D and G bands of carbon, respectively, indicating the presence of the carbon component in the composite [22,31]. The high I_G/I_D intensity ratio (1.05) reveals good graphitization degree of the carbon substrate, which is favorable for enhancing the electrical conductivity of the MoS_2/C composites [2,32].

The composition and chemical states of the as-prepared MoS_2@carbon were characterized by X-ray photoelectron spectroscopy (XPS). The survey spectrum in Figure 2a indicates the existence of main elements of C, Mo, and S as well as a trace of O element absorbed on the surface [33]. The core level spectrum of Mo 3d (Figure 2b) and S 2p (Figure 2c) show characteristic peaks with binding energies located at 232.6, 229.5, 163.5, and 162.2 eV, which belong to the Mo $3d_{3/2}$, Mo $3d_{5/2}$, S $2p_{1/2}$, and S $2p_{3/2}$ components of MoS_2, respectively [34,35]. The C 1s XPS peak (Figure 2d) can be fitted C–C and C–O–C components. All these results reveal the successful preparation of MoS_2 on the carbon fiber [23].
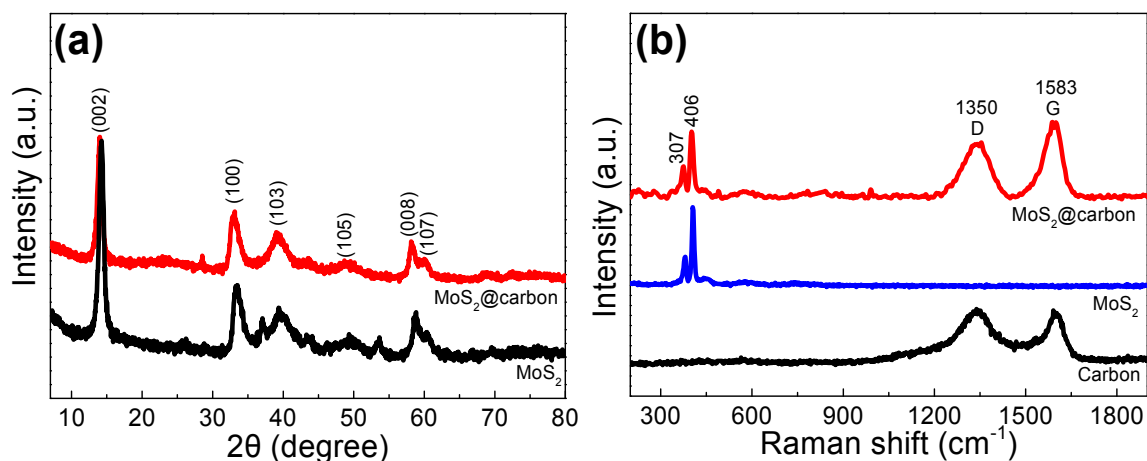
Figure 1. (**a**) XRD patterns of the as-prepared MoS_2@carbon, pure MoS_2; (**b**) Raman spectra of the as-prepared MoS_2@carbon, pure MoS_2, and the carbon substrate.
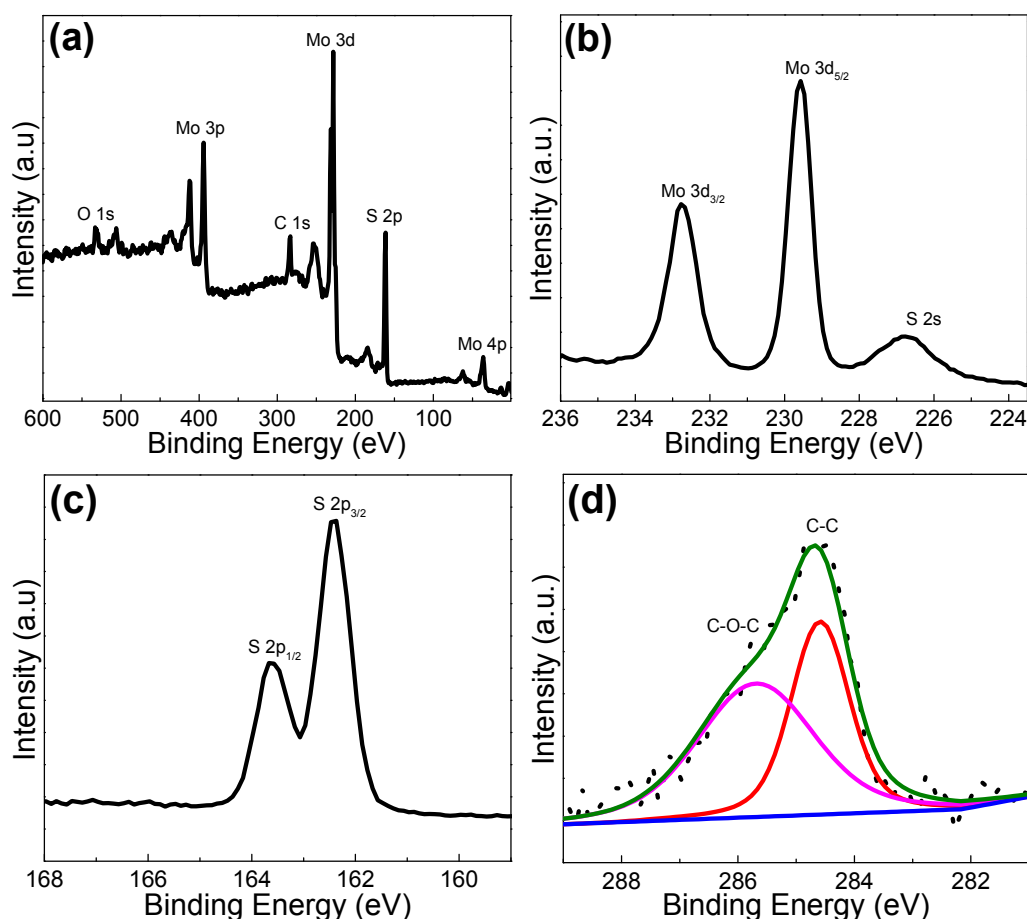

Figure 2. XPS spectra of MoS_2@carbon composite fiber membranes: (**a**) the survey scan; (**b**) Mo 3d; (**c**) S 2p; (**d**) C 1s.

Figure 3 shows the field-emission scanning electron microscopy (SEM) and transmission electron microscopy (TEM) images of the pure carbon and MoS_2@carbon composites. Figure 3a exhibits the typical morphology of pure cotton-derived carbon substrate, which is composed of one-dimensional (1D) fibers with smooth surface (inset) and an average diameter of 7 μm. In addition, the carbon fibers form a randomly-entangled 3D network, which is favorable for solution flux and thus uniform

growth of MoS$_2$. Figure 3b shows a panoramic view of the MoS$_2$@carbon composites, which inherit the 1D fibrous morphology of carbon substrates. Figure 3c shows the uniform and conformal deposition of MoS$_2$ nanostructures on the carbon surface, thus constructing coaxial configuration. The higher-resolution SEM image (inset in Figure 3c) reveals porous MoS$_2$ nanosheets aligned vertically on the fiber surface. The 1D/2D hierarchical architecture of the MoS$_2$@carbon composites is beneficial for electrolyte penetration, and enlarges electrode/electrolyte interface area. The TEM image in Figure 3e exhibits ultrathin nanosheet-like MoS$_2$ structures [36]. The high-resolution TEM (HRTEM) image in Figure 3f shows a typical edge view of the MoS$_2$ nanosheets with clear lattice fringes. The thickness of the MoS$_2$ nanosheets is estimated to be about 10 nm, and the interlayer spacing of 0.65 nm corresponds to the (002) plane of the MoS$_2$ [37]. For comparison, pure MoS$_2$ nanoflowers with an average diameter of 500 nm were prepared as a control sample (Figure 3d).
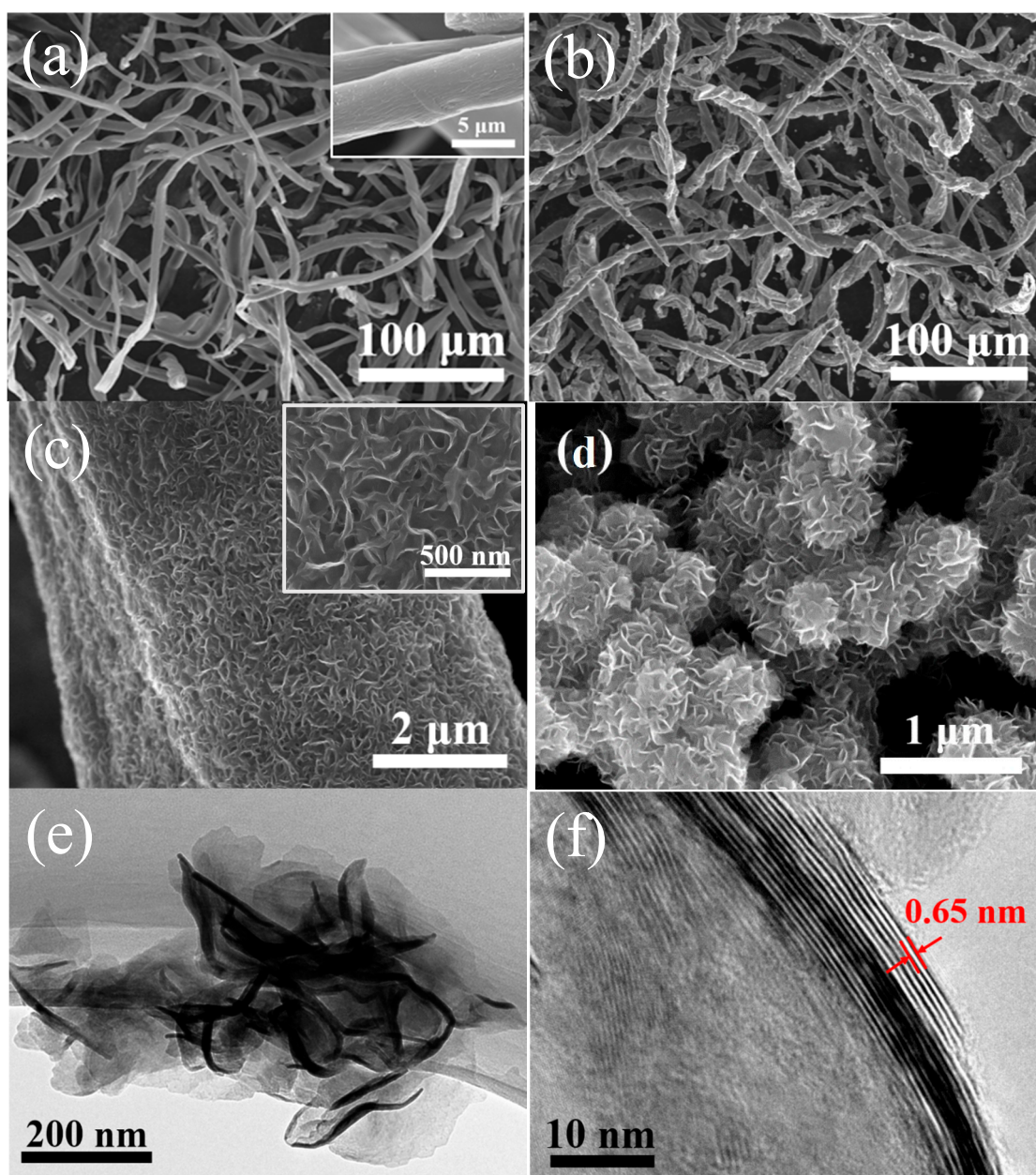

Figure 3. (**a**) Field emission scanning electron microscopy (SEM) image of pure cotton-derived carbon; (**b**,**c**) SEM images; (**e**) high-magnification transmission electron microscopy (TEM) image; and (**f**) high-resolution TEM (HRTEM) image of MoS$_2$@carbon; (**d**) SEM image of pure MoS$_2$.
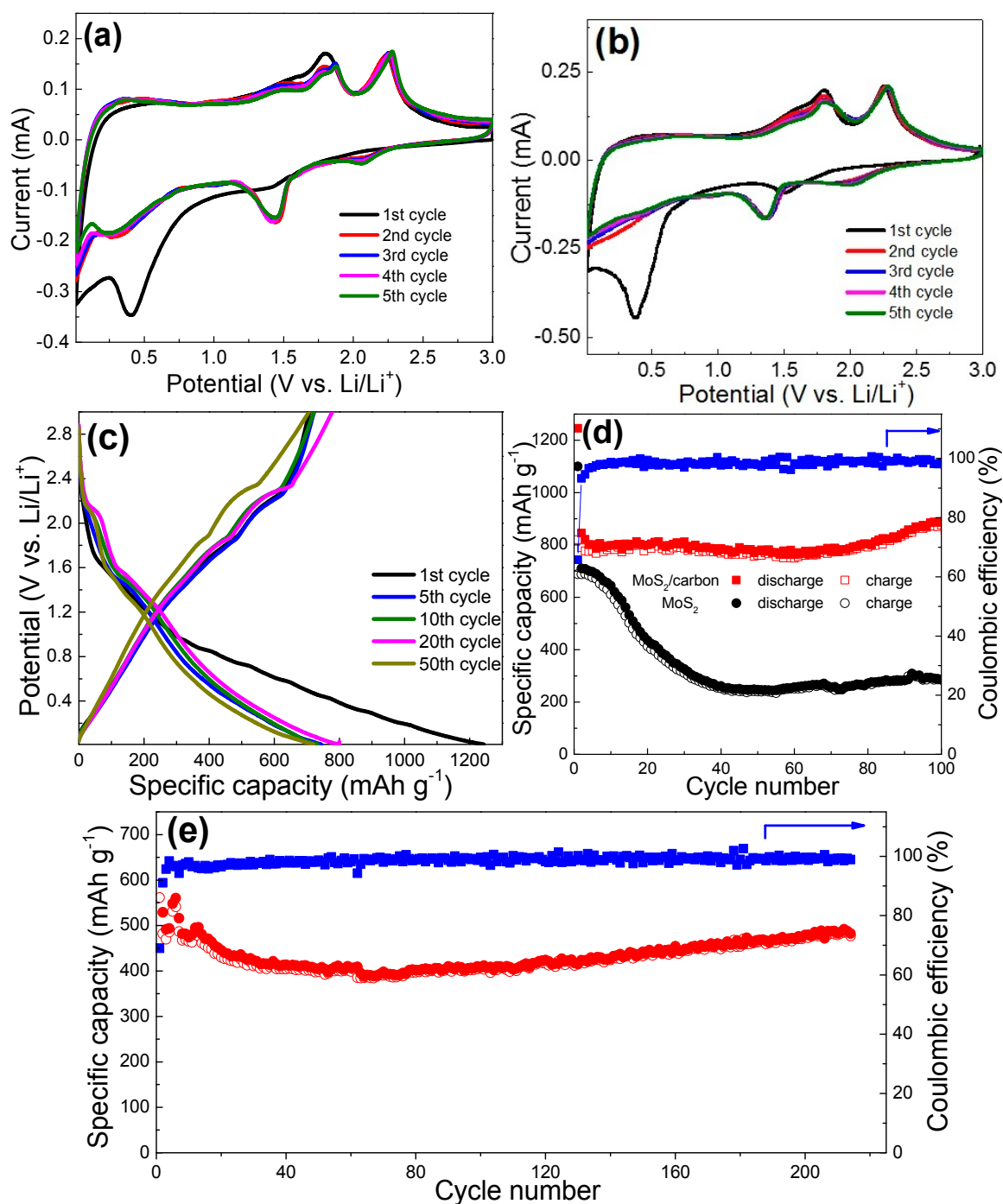
Figure 4. Cyclic voltammetry (CV) curves of the (**a**) MoS$_2$@carbon and (**b**) pure MoS$_2$ electrodes at 0.1 mV·s^{-1}; (**c**) charge–discharge curves of the MoS$_2$@carbon at 100 mA·g^{-1}. Cycling performance and the coulombic efficiencies of the electrodes tested at (**d**) 100 mA·g^{-1} and (**e**) 2000 mA·g^{-1}.

To evaluate electrochemical properties, the MoS$_2$@carbon composite was investigated as an anode material for lithium-ion batteries. As shown in Figure 4a,b, the MoS$_2$@carbon composite electrode shares identical CV curve shapes to pure MoS$_2$ electrodes for the initial five cycles at a scanning rate of 0.1 mV·s^{-1} in the potential range of 0.01–3.0 V (versus Li/Li$^+$). Specifically, in the first cycle, there are two cathodic peaks appearing at about 1.5 V and 0.35 V. The broad peak at about 1.5 V corresponds to Li$^+$ intercalation into the layered structure of the MoS$_2$ to form Li$_x$MoS$_2$. The 0.35 V peak is attributed to the further conversion reaction from Li$_x$MoS$_2$ into metallic Mo and Li$_2$S [18,31,38]. In the reverse

anodic scan, the oxidation peaks at 1.8 V and 2.3 V are associated with the stepwise oxidation of Mo into Mo^{4+}/Mo^{6+} and the oxidation of Li_2S into sulfur or polysulfides, respectively [39]. In the subsequent cycles, the reduction peaks at 1.4 V and 2 V are ascribed to the reduction of Mo^{6+}/Mo^{4+} and the formation of Li_2S, respectively. Galvanostatic charge/discharge cycling measurements were carried out to investigate the lithium storage capacity of the MoS_2@carbon composites. As shown in Figure 4c, two voltage plateaus at 1.5 V and 0.35 V are observed in the first discharge curve, indicating the two-step lithiation reaction of MoS_2. In the following discharge curves, the plateaus observed in the first discharge shift towards the higher potentials of 2 V and 1.4 V due to the improved reaction kinetics after the first lithiation. During the charging process, the MoS_2@carbon composite shows two potential plateaus around 1.8 V and 2.3 V, which are consistent with the CV curves [22,40]. Figure 4d presents the cyclic performance of the as-prepared MoS_2@carbon composites and pure MoS_2 powders at a current density of 100 $mA \cdot g^{-1}$. It can be seen that the MoS_2@carbon anode delivers an initial discharge and charge capacities of 1246 and 820 $mAh \cdot g^{-1}$, respectively, which are higher than those of the pure MoS_2 electrode (i.e., 1100 and 689 $mAh \cdot g^{-1}$) and comparable to the reported MoS_2/graphene (i.e., 1160 and 896 $mAh \cdot g^{-1}$) [41]. The initial capacity loss is mainly caused by the irreversible processes such as the inevitable formation of a solid–electrolyte interface (SEI) film on the electrode surface and some side reactions between Li^+ and active materials [42–46]. The Coulombic efficiency is as high as 67.6% in the first cycle (vs. 62.6% for the pure MoS_2), which increases to >98% from the second cycles. More importantly, the composite anode retains a high specific capacity of 869 $mAh \cdot g^{-1}$ after 100 cycles, indicating excellent cycling stability. For comparison, the specific capacity of the pure MoS_2 electrode decreases significantly to only 290 $mAh \cdot g^{-1}$ after 100 cycles. In addition, the good cyclic performance of the MoS_2@carbon composite is further confirmed by another cell tested at a current density of 2000 $mA \cdot g^{-1}$. As shown in Figure 4e, the composite electrode can deliver a reversible specific capacity of about 480 $mAh \cdot g^{-1}$ after 210 cycles, which is still higher than the commercial graphite anode (372 $mAh \cdot g^{-1}$).
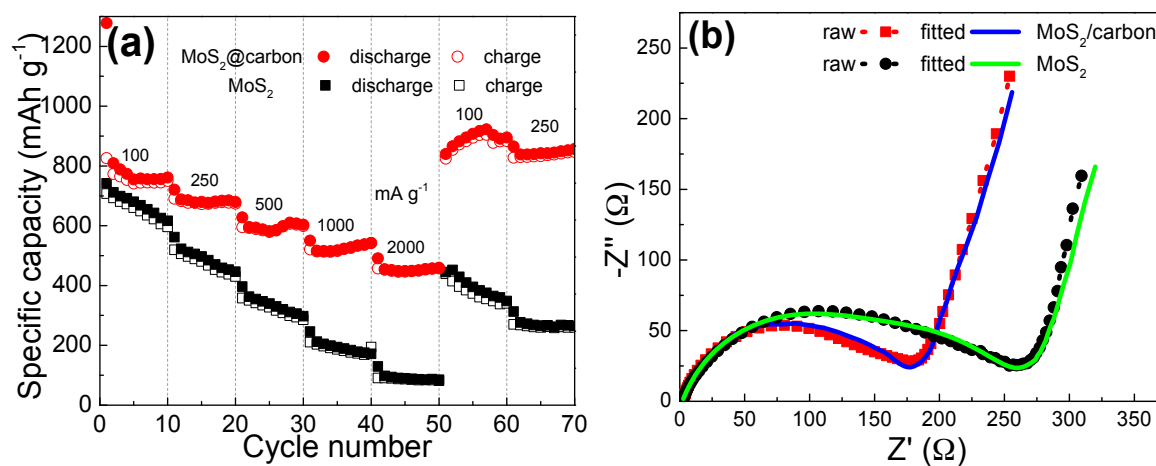
Figure 5. (**a**) Rate performance; and (**b**) electrochemical impedance spectra (EIS) of the MoS_2@carbon and MoS_2 powders.

In addition to the higher specific capacity and cyclic performance, the MoS_2@carbon anode also exhibits enhanced rate capability compared to the pure MoS_2 powder. Figure 5a compares the rate performance of the anodes. When the current density increases gradually from 100 to 2000 $mA \cdot g^{-1}$, the MoS_2@carbon anode can maintain a reversible specific capacity of 457 $mAh \cdot g^{-1}$, revealing its excellent rate capability. As the current density returns to 100 and 250 $mA \cdot g^{-1}$, the composite anode recovers its average specific capacities of 891 and 840 $mAh \cdot g^{-1}$, again indicating the outstanding reversibility of the MoS_2@carbon anode. In sharp contrast, the MoS_2 powder anode merely delivered about 85 $mAh \cdot g^{-1}$ at 2000 $mA \cdot g^{-1}$. The better rate capability of the MoS_2@carbon anode can be

ascribed to the conductive carbon substrate, which offers high conductivity for rapid electron collection and transfer. A better understanding of the resistive behavior is gained from the electrochemical impedance spectra (EIS). Figure 5b shows the resulting Nyquist plots fitted by Zview software. The EIS curves of both electrodes are composed of one semicircle in the high-to-mediate frequency region and a spike in the low-frequency region. The semicircle corresponds to the charge transfer resistance (R_{ct}), and the spike is associated with the Li-ion diffusion into the electrode [41]. Notably, the MoS_2@carbon anode shows a smaller R_{ct} than the pure MoS_2 anode (175 vs. 260 Ω). The decreased R_{ct} reveals that the combination of carbon and MoS_2 components renders improved reaction kinetics for fast electrochemical reactions.

Combining the high specific capacity, good rate capability, and excellent cycling stability, the MoS_2@carbon composite could serve as a low-cost anode material with attractive electrochemical properties. The performance enhancement of the composite could be attributed to the unique hierarchical coaxial configuration [42,47]. First, the bio-mass-derived 1D carbon fiber substrate offers high conducting pathways for fast electron transfer, while the MoS_2 nanostructures shorten the electron transport distances. In addition, the 3D scaffold and the porous MoS_2 nanosheets facilitate smooth electrolyte penetration and ion transport. Both the enhanced electron and ion transport would accelerate the reaction kinetics and thus improve the electrochemical utilization of the composite. Second, the nanoscaled size and uniform distribution of the MoS_2 nanosheets on the carbon fibers enlarge the contact area between MoS_2 and electrolyte, thereby offering more active sites for Li-ion storage. Third, the coverage of MoS_2 on carbon can help to reduce the carbon–electrolyte interaction and reduce side reactions responsible for the irreversible capacity. Fourth, the carbon matrix provides a solid backbone to prevent MoS_2 nanosheets from restacking and agglomeration during the charge/discharge processes, which ensures the structural integrity of the whole electrode for long-term cycling endurance.

3. Materials and Methods

3.1. Synthesis of the MoS_2@Carbon Composites

All reagents were of analytical grade and used as received without further purification. In a typical procedure, natural cotton was employed as a biomass source of the carbon substrate. The cotton was first carbonized at 900 °C for 3 h (heating rate: 5 °C/min) under N_2 atmosphere in a horizontal tube furnace to obtain carbon. Subsequently, MoS_2@carbon composites were synthesized using the one-step hydrothermal method. Typically, 0.076 g of ammonium molybdate tetrahydrate ((NH_4)$_6$$Mo_7O_{24}$·$4H_2O$, AMT) and 1 g of thiourea was dissolved in 35 mL deionized water under magnetic stirring for 30 min. Then, 100 mg of the carbon substrate was immersed into the solution, which was transferred into a 50 mL Teflon-lined stainless steel autoclave and kept at 180 °C for 24 h. After cooling down to room temperature, the black product was washed with deionized water and ethanol several times, and finally dried at 60 °C for 12 h. MoS_2@carbon was calcined at 800 °C for 2 h under N_2 atmosphere to increase the degree of crystallinity. For comparison, MoS_2 powder was synthesized via the same hydrothermal procedure but without the addition of carbon.

3.2. Material Characterization

The phase structure of the samples was characterized by X-ray diffraction (XRD) with Cu Kα radiation (λ = 0.15418 nm) (X'Pert Pro MPD, Philips, Almelo, The Netherlands). Raman spectral analysis was carried out on a Renishaw inVia Raman Spectrometer (Renishaw Invia RM200, London, UK) using an excitation wavelength of 532 nm. The as-prepared sample was placed on conductive resin to observe the morphology using field emission scanning electron microscopy (FE-SEM, FEI Nano SEM 450, FEI, Portland, OR, USA). The composite was dispersed in ethanol under ultrasonication for transmission electron microscopy (TEM, FEI Tecnai F30G^2, FEI, Portland, OR, USA) investigation.

The surface elements and chemical states of the sample were examined by X-ray photoelectron spectroscopy (XPS, ESCALAB 250Xi, Thermo Scientific, Waltham, MA, USA).

3.3. Electrochemical Measurements

The electrochemical performance was evaluated using CR 2016 coin cells assembled in an argon-filled glove box. The working electrode was fabricated by casting a slurry of 70 wt % active material, 20 wt % conductive agent (carbon black), and 10 wt % binder (polyvinylidene fluoride) in N-methyl-2-pyrrolidinone (NMP) on a copper foil. Li foil, a Celgard 2400 microporous polypropylene membrane, and a solution of 1M $LiPF_6$ in ethylene carbonate (EC), dimethyl carbonate (DMC), and ethylmethyl carbonate (EMC) (1:1:1, volume ratio) served as the counter electrode, the separator, and the electrolyte, respectively. Solartron electrochemical workstation (1260 + 1287, Bognor Regis, UK) was employed to obtain the cyclic voltammetry (CV) in the potential range of 0.01–3.0 V (vs. Li/Li$^+$) at a rate of 0.1 mV·s^{-1}, and the electrochemical impedance spectra (EIS) in the frequency range from 1 MHz to 50 mHz. Galvanostatic charge/discharge cycling was conducted on a Land battery system (LAND, BT2013A, Wuhan, China) under different current densities.

4. Conclusions

A low-cost bio-mass-derived carbon material was explored as effective substrates for the uniform growth of MoS_2 nanosheets via a hydrothermal approach. The MoS_2@carbon composite exhibits well-defined 1D/2D hierarchical coaxial architecture, which is favorable for improving the reaction kinetics and the electrode structure. When evaluated as an anode of LIBs, the MoS_2@carbon composite delivers a high specific capacity of 820 mAh·g^{-1} at 100 mA·g^{-1}, superior rate capability with 457 mAh·g^{-1} retained at a high-rate current of 2000 mA·g^{-1}, and excellent cycling stability without noticeable capacity loss after 100 cycles. The remarkable lithium ion storage performance makes the present MoS_2@carbon composite a promising low-cost anode material candidate for high-performance LIBs.

Author Contributions: Jian-Gan Wang and Rui Zhou conceived and designed the experiments; Rui Zhou, Hongzhen Liu, Huanyan Liu, and Dandan Jin performed the experiments; Jian-Gan Wang, Rui Zhou, Xingrui Liu, Chao Shen, Keyu Xie, and Bingqing Wei analyzed the results; Jian-Gan Wang, Rui Zhou, and Bingqing Wei co-wrote this paper.

Conflicts of Interest: The authors declare no conflict of interest.

References

1. Nitta, N.; Wu, F.; Lee, J.T.; Yushin, G. Li-ion battery materials: Present and future. *Mater. Today* **2015**, *18*, 252–264. [CrossRef]

2. Wang, J.-G.; Jin, D.; Zhou, R.; Li, X.; Liu, X.R.; Shen, C.; Xie, K.; Li, B.; Kang, F.; Wei, B. Highly flexible graphene/Mn_3O_4 nanocomposite membrane as advanced anodes for Li-ion batteries. *ACS Nano* **2016**, *10*, 6227–6234. [CrossRef] [PubMed]

3. Wang, J.-G.; Jin, D.; Liu, H.; Zhang, C.; Zhou, R.; Shen, C.; Xie, K.; Wei, B. All-manganese-based Li-ion batteries with high rate capability and ultralong cycle life. *Nano Energy* **2016**, *22*, 524–532. [CrossRef]

4. Reddy, M.V.; Subba Rao, G.V.; Chowdari, B.V. Metal oxides and oxysalts as anode materials for Li ion batteries. *Chem. Rev.* **2013**, *113*, 5364–5457. [CrossRef] [PubMed]

5. Xu, B.; Qian, D.; Wang, Z.; Meng, Y.S. Recent progress in cathode materials research for advanced lithium ion batteries. *Mat. Sci. Eng. R* **2012**, *73*, 51–65. [CrossRef]

6. Wang, J.; Hou, X.; Zhang, M.; Li, Y.; Wu, Y.; Liu, X.; Hu, S. 3-aminopropyltriethoxysilane-assisted Si@SiO$_2$/CNTs hybrid microspheres as superior anode materials for Li-ion batteries. *Silicon* **2016**, *9*, 97–104. [CrossRef]

7. Sun, Y.-H.; Liu, S.; Zhou, F.-C.; Nan, J.-M. Electrochemical performance and structure evolution of core-shell nano-ring α-Fe$_2$O$_3$@carbon anodes for lithium-ion batteries. *Appl. Surf. Sci.* **2016**, *390*, 175–184. [CrossRef]

8. Wang, J.-G.; Zhang, C.; Jin, D.; Xie, K.; Wei, B. Synthesis of ultralong MnO/C coaxial nanowires as freestanding anodes for high-performance lithium ion batteries. *J. Mater. Chem. A* **2015**, *3*, 13699–13705. [CrossRef]

9. Ramakrishna Matte, H.S.S.; Gomathi, A.; Manna, A.K.; Late, D.J.; Datta, R.; Pati, S.K.; Rao, C.N.R. MoS$_2$ and WS$_2$ analogues of graphene. *Angew. Chem. Int. Ed.* **2010**, *122*, 4153–4156. [CrossRef]

10. Bhandavat, R.; David, L.; Singh, G. Synthesis of surface-functionalized WS$_2$ nanosheets and performance as li-ion battery anodes. *J. Phys. Chem. Lett.* **2012**, *3*, 1523–1530. [CrossRef] [PubMed]

11. Wang, Q.; Zou, R.; Xia, W.; Ma, J.; Qiu, B.; Mahmood, A.; Zhao, R.; Yang, Y.; Xia, D.; Xu, Q. Facile synthesis of ultrasmall CoS$_2$ nanoparticles within thin N-doped porous carbon shell for high performance lithium-ion batteries. *Small* **2015**, *11*, 2511–2517. [CrossRef] [PubMed]

12. Yu, L.; Yang, J.F.; Lou, X.W. Formation of CoS$_2$ nanobubble hollow prisms for highly reversible lithium storage. *Angew. Chem. Int. Ed.* **2016**, *55*, 13422–13426. [CrossRef] [PubMed]

13. Tan, C.; Zhang, H. Two-dimensional transition metal dichalcogenide nanosheet-based composites. *Chem. Soc. Rev.* **2015**, *44*, 2713–2731. [CrossRef] [PubMed]

14. Jin, B.; Zhou, X.; Huang, L.; Licklederer, M.; Yang, M.; Schmuki, P. Aligned MoO$_x$/MoS$_2$ core-shell nanotubular structures with a high density of reactive sites based on self-ordered anodic molybdenum oxide nanotubes. *Angew. Chem. Int. Ed.* **2016**, *55*, 12252–12256. [CrossRef] [PubMed]

15. Hu, S.; Chen, W.; Zhou, J.; Yin, F.; Uchaker, E.; Zhang, Q.; Cao, G. Preparation of carbon coated MoS$_2$ flower-like nanostructure with self-assembled nanosheets as high-performance lithium-ion battery anodes. *J. Mater. Chem. A* **2014**, *2*, 7862–7872. [CrossRef]

16. Stephenson, T.; Li, Z.; Olsen, B.; Mitlin, D. Lithium ion battery applications of molybdenum disulfide (MoS$_2$) nanocomposites. *Energy Environ. Sci.* **2014**, *7*, 209–231. [CrossRef]

17. Xiong, F.; Cai, Z.; Qu, L.; Zhang, P.; Yuan, Z.; Asare, O.K.; Xu, W.; Lin, C.; Mai, L. Three-dimensional crumpled reduced graphene oxide/MoS$_2$ nanoflowers: A stable anode for lithium-ion batteries. *ACS Appl. Mater. Inter.* **2015**, *7*, 12625–12630. [CrossRef] [PubMed]

18. Xie, D.; Wang, D.H.; Tang, W.J.; Xia, X.H.; Zhang, Y.J.; Wang, X.L.; Gu, C.D.; Tu, J.P. Binder-free network-enabled MoS$_2$-ppy-rGO ternary electrode for high capacity and excellent stability of lithium storage. *J. Power Sources* **2016**, *307*, 510–518. [CrossRef]

19. Jeong, J.M.; Lee, K.G.; Chang, S.J.; Kim, J.W.; Han, Y.K.; Lee, S.J.; Choi, B.G. Ultrathin sandwich-like MoS$_2$@N-doped carbon nanosheets for anodes of lithium ion batteries. *Nanoscale* **2015**, *7*, 324–329. [CrossRef] [PubMed]

20. Liu, Y.; He, X.; Hanlon, D.; Harvey, A.; Khan, U.; Li, Y.; Coleman, J.N. Electrical, mechanical, and capacity percolation leads to high-performance MoS$_2$/nanotube composite lithium ion battery electrodes. *ACS Nano* **2016**, *10*, 5980–5990. [CrossRef] [PubMed]

21. Liu, Y.; Zhao, Y.; Jiao, L.; Chen, J. A graphene-like MoS$_2$/graphene nanocomposite as a high performance anode for lithium ion batteries. *J. Mater. Chem. A* **2014**, *2*, 13109. [CrossRef]

22. Li, H.; Yu, K.; Fu, H.; Guo, B.; Lei, X.; Zhu, Z. MoS$_2$/graphene hybrid nanoflowers with enhanced electrochemical performances as anode for lithium-ion batteries. *J. Phys. Chem. C* **2015**, *119*, 7959–7968. [CrossRef]

23. Zhu, C.; Mu, X.; van Aken, P.A.; Yu, Y.; Maier, J. Single-layered ultrasmall nanoplates of MoS$_2$ embedded in carbon nanofibers with excellent electrochemical performance for lithium and sodium storage. *Angew. Chem. Int. Ed.* **2014**, *53*, 2152–2156. [CrossRef] [PubMed]

24. Kong, J.; Zhao, C.; Wei, Y.; Lu, X. MoS$_2$ nanosheets hosted in polydopamine-derived mesoporous carbon nanofibers as lithium-ion battery anodes: Enhanced MoS$_2$ capacity utilization and underlying mechanism. *ACS Appl. Mater. Inter.* **2015**, *7*, 24279–24287. [CrossRef] [PubMed]

25. Bian, X.; Zhu, J.; Liao, L.; Scanlon, M.D.; Ge, P.; Ji, C.; Girault, H.H.; Liu, B. Nanocomposite of MoS$_2$ on ordered mesoporous carbon nanospheres: A highly active catalyst for electrochemical hydrogen evolution. *Electrochem. Commu.* **2012**, *22*, 128–132. [CrossRef]

26. Xie, X.; Ao, Z.; Su, D.; Zhang, J.; Wang, G. MoS$_2$/graphene composite anodes with enhanced performance for sodium-ion batteries: The role of the two-dimensional heterointerface. *Adv. Func. Mater.* **2015**, *25*, 1393–1403. [CrossRef]

27. Qu, Q.; Qian, F.; Yang, S.; Gao, T.; Liu, W.; Shao, J.; Zheng, H. Layer-by-layer polyelectrolyte assisted growth of 2D ultrathin MoS$_2$ nanosheets on various 1D carbons for superior Li-storage. *ACS Appl. Mater. Int.* **2016**, *8*, 1398–1405. [CrossRef] [PubMed]

28. Xie, X.; Makaryan, T.; Zhao, M.; van Aken, K.L.; Gogotsi, Y.; Wang, G. MoS$_2$ nanosheets vertically aligned on carbon paper: A freestanding electrode for highly reversible sodium-ion batteries. *Adv. Energy Mater.* **2016**, *6*, 1502161. [CrossRef]

29. Li, Y.; Wang, H.; Xie, L.; Liang, Y.; Hong, G.; Dai, H. MoS$_2$ nanoparticles grown on graphene: An advanced catalyst for the hydrogen evolution reaction. *J. Am. Chem. Soc.* **2011**, *133*, 7296–7299. [CrossRef] [PubMed]

30. Zhou, J.; Qin, J.; Zhang, X.; Shi, C.; Liu, E.; Li, J.; Zhao, N.; He, C. 2D space-confined synthesis of few-layer MoS$_2$ anchored on carbon nanosheet for lithium-ion battery anode. *ACS Nano* **2015**, *9*, 3837–3848. [CrossRef] [PubMed]

31. Shan, T.; Xin, S.; You, Y.; Cong, H.; Yu, S. Arumugam Manthiram. Combining nitrogen-doped graphene sheets and MoS$_2$: A unique film–foam–film structure for enhanced lithium storage. *Angew. Chem. Int. Ed.* **2016**, *55*, 1–7. [CrossRef] [PubMed]

32. Wang, J.-G.; Kang, F.; Wei, B. Engineering of MnO$_2$-based nanocomposites for high performance supercapacitors. *Prog. Mater. Sci.* **2015**, *74*, 51–124. [CrossRef]

33. Zhu, H.; Lyu, F.; Du, M.; Zhang, M.; Wang, Q.; Yao, J.; Guo, B. Design of two-dimensional ultrathin MoS$_2$ nanoplates fabricated within one-dimensional carbon nanofibers with thermosensitive morphology: High-performance electrocatalysts for the hydrogen evolution reaction. *ACS Appl. Mater. Int.* **2014**, *6*, 22126–22137. [CrossRef] [PubMed]

34. Ramkumar, M.; Minakshi, M. A biopolymer gel-decorated cobalt molybdate nanowafer: Effective graft polymer cross-linked with an organic acid for better energy storage. *New J. Chem.* **2016**, *44*, 2863–2877. [CrossRef]

35. Barmi, M.J.; Minakshi, M. Tuning the Redox Properties of the Nanostructured CoMoO$_4$ Electrode: Effects of Surfactant Content and Synthesis Temperature. *ChemPlusChem* **2016**, *81*, 964–977. [CrossRef]

36. Ramkumar, M.; Minakshi, M. Fabrication of ultrathin CoMoO$_4$ nanosheets modified with chitosan and their improved performance in energy storage device. *Dalton Trans.* **2015**, *44*, 6158–6168. [CrossRef] [PubMed]

37. Fang, Y.; Lv, Y.; Gong, F.; Elzatahry, A.A.; Zheng, G.; Zhao, D. Synthesis of 2D-mesoporous-carbon/MoS$_2$ heterostructures with well-defined interfaces for high-performance lithium-ion batteries. *Adv. Mater.* **2016**, *28*, 9385–9390. [CrossRef] [PubMed]

38. Jiang, L.; Lin, B.; Li, X.; Song, X.; Xia, H.; Li, L.; Zeng, H. Monolayer MoS$_2$-graphene hybrid aerogels with controllable porosity for lithium-ion batteries with high reversible capacity. *ACS Appl. Mater. Int.* **2016**, *8*, 2680–2687. [CrossRef]

39. Zhou, F.; Xin, S.; Liang, H.W.; Song, L.T.; Yu, S.H. Carbon nanofibers decorated with molybdenum disulfide nanosheets: Synergistic lithium storage and enhanced electrochemical performance. *Angew. Chem. Int. Ed.* **2014**, *53*, 11552–11556. [CrossRef] [PubMed]

40. Zuo, X.; Chang, K.; Zhao, J.; Xie, Z.; Tang, H.; Li, B.; Chang, Z. Bubble-template-assisted synthesis of hollow fullerene-like MoS$_2$ nanocages as a lithium ion battery anode material. *J. Mater. Chem. A* **2016**, *4*, 51–58. [CrossRef]

41. Teng, Y.; Zhao, H.; Zhang, Z.; Li, Z.; Xia, Q.; Zhang, Y.; Zhao, L.; Du, X.; Du, Z.; Lv, P.; Świerczek, K. MoS$_2$ Nanosheets vertically grown on graphene sheets for lithium-ion battery anodes. *ACS Nano* **2016**, *10*, 8526–8535. [CrossRef] [PubMed]

42. Xu, X.; Fan, Z.; Yu, X.; Ding, S.; Yu, D.; Lou, X. A nanosheets-on-channel architecture constructed from MoS$_2$ and CMK-3 for high-capacity and long-cycle-life lithium storage. *Adv. Energy Mater.* **2014**, *4*, 1400902. [CrossRef]

43. Chang, K.; Chen, W. L-cysteine-assisted synthesis of layered MoS$_2$/graphene composites with excellent electrochemical performances for lithium ion batteries. *ACS Nano* **2011**, *5*, 4720–4728. [CrossRef] [PubMed]

44. Ji, L.; Lin, Z.; Alcoutlabi, M.; Zhang, X. Recent developments in nanostructured anode materials for rechargeable lithium-ion batteries. *Energy Environ. Sci.* **2011**, *4*, 2682–2699.

45. Agubra, V.A.; Zuniga, L.; Garza, D.D.; Gallegos, L.; Pokhrel, M.; Alcoutlabi, M. Forcespinning: A new method for the mass production of Sn/C composite nanofiber anodes for lithium ion batteries. *Solid State Ion.* **2016**, *286*, 72–82. [CrossRef]

46. Agubra, V.A.; Zuniga, L.; Flores, D.; Villareal, J.; Alcoutlabi, M. Composite nanofibers as advanced materials for Li-ion, Li-O_2 and Li-S batteries. *Electrochim. Acta* **2016**, *192*, 529–550. [CrossRef]

47. Li, J.-C.; Hou, P.X.; Zhao, S.Y.; Liu, C.; Tang, D.M.; Cheng, M.; Zhang, F.; Cheng, H.M. A 3D bi-functional porous N-doped carbon microtube sponge electrocatalyst for oxygen reduction and oxygen evolution reactions. *Energy Environ. Sci.* **2016**, *9*, 3079–3084. [CrossRef]